



**NAVAL
POSTGRADUATE
SCHOOL**

MONTEREY, CALIFORNIA

THESIS

**CHARACTERIZATION OF MEMS A DIRECTIONAL MICROPHONE
WITH SOLID AND PERFORATED WINGS**

by

Norbahrin Muamad

June 2009

Thesis Adviser:
Co-Adviser:

Gamani Karunasiri
Bruce Denardo

Approved for public release; distribution is unlimited

THIS PAGE INTERNATIONALLY LEFT BLANK

REPORT DOCUMENTATION PAGE		From Approved OMB No. 0704-0188	
Public reporting burden for this collection of information is estimated to average 1 hour per response, including the time for reviewing instruction searching existing data sources, gathering and maintaining the data needed, and completing and reviewing the collection of information. Send comments regarding this burden estimate or any other aspect of this collection of information, including suggestion for reducing this burden, to Washington headquarters Service, Directorate for Information Operations and Reports, 1215 Jefferson David Highway, Suite 1204, Arlington, VA 22202-4302, and to the Office of Management and Budget, Paperwork Reduction Project (0704-0188) Washington DC 20503.			
1. AGENCY USE ONLY (Leave blank)	2. REPORT DATE June 2009	3. REPORT TYPE AND DATES COVERED Master's Thesis	
4. TITLE AND SUBTITLE Characterization of MEMS a Directional Microphone with Solid and Perforated Wings		5. FUNDING NUMBERS	
6. AUTHOR(S) Norbahrin Muamad		8. PERFORMING ORGANIZATION REPORT NUMBER	
7. PERFORMING ORGANIZATION NAME(S) AND ADDRESS(ES) Naval Postgraduate School Monterey, CA 93943-5000		10. SPONSORING/MONITORING AGENCY REPORT NUMBER	
9. SPONSORING/MONITORING AGENCY NAME(S) AND ADDRESS(ES) N/A		11. SUPPLEMENTARY NOTES The views expressed in this thesis are those of the author and do not reflect the official policy or position of the Department of Defense or the U.S. Government.	
12a. DISTRIBUTION/AVAILABILITY STATEMENT Approved for public release; distribution unlimited		12.b. DISTRIBUTION CODE	
13. ABSTRACT (maximum 200 words) This goal of this research is to characterize two micro electro mechanical system (MEMS) based directional sound sensors with solid and perforated wings. The design of the sensors was based on the structure of <i>Ormia ochracea</i> fly's hearing system that has highly directional hearing through mechanical coupling of the eardrums. The sensors are made of 10 micron thick single crystal silicon layer with dimensions 1 x 2 mm ² . The sensors were fabricated using SOIMUMPs process available through MEMSCAP foundry service. The characteristics of the two sensors were simulated COMSOL finite element software and responses to incident sound at different angles were measured using a laser vibrometer. Both sensors showed good sound coupling and measured and simulated frequency responses are in good agreement. The sensor with perforated wings was found to have faster response compared with that of the solid wings primarily due to lower mass and higher damping. The measurements showed good sensitivity to the direction of sound as predicted from the modeling.			
14. SUBJECT TERMS SOIMUMPs, MEMS, Ormia Ochracea, Biomimetic, Directional Microphone, Sensor, Microphone, Fly Hearing, Undersea Warfare		15. NUMBER OF PAGES 57	
		16. PRICE CODE	
17. SECURITY CLASSIFICATION OF REPORT Unclassified	18. SECURITY CLASSIFICATION OF THIS PAGE Unclassified	19. SECURITY CLASSIFICATION OF ABSTRACT Unclassified	20. LIMITATION OF ABSTRACT UU

NSN 7540-01-280-5500

Standard Form 298 (Rev. 2-89)
Prescribed by ANSI Std. Z39-18

THIS PAGE INTERNATIONALLY LEFT BLANK

Approved for public release: distribution unlimited

**CHARACTERIZATION OF MEMS A DIRECTIONAL MICROPHONE WITH
SOLID AND PERFORATED WINGS**

Norbahrin Muamad
Major, Royal Brunei Navy
BEng in Electronic Engineering, Salford University, 2000

Submitted in partial fulfillment of the
requirement for the degree of

MASTER OF SCIENCE IN APPLIED PHYSICS

from the

NAVAL POSTGRADUATE SCHOOL

June 2009

Author: Norbahrin Muamad

Approved by: Gamani Karunasiri
Thesis Advisor

Bruce Denardo
Thesis Co-Advisor

James H. Luscombe
Chairman, Department of Physics

THIS PAGE INTERNATIONALLY LEFT BLANK

ABSTRACT

This goal of this research is to characterize two micro electro mechanical system (MEMS) based directional sound sensors with solid and perforated wings. The design of the sensors was based on the structure of *Ormia ochracea* fly's hearing system that has highly directional hearing through mechanical coupling of the eardrums. The sensors are made of 10 micron thick single crystal silicon layer with dimensions 1 x 2 mm². The sensors were fabricated using SOIMUMPs process available through MEMSCAP foundry service. The characteristics of the two sensors were simulated COMSOL finite element software and responses to incident sound at different angles were measured using a laser vibrometer. Both sensors showed good sound coupling and measured and simulated frequency responses are in good agreement. The sensor with perforated wings was found to have faster response compared with that of the solid wings primarily due to lower mass and higher damping. The measurements showed good sensitivity to the direction of sound as predicted from the modeling.

THIS PAGE INTENTIONALLY LEFT BLANK

TABLE OF CONTENTS

I.	INTRODUCTION.....	1
A.	INTRODUCTION.....	1
B.	BACKGROUND.....	2
C.	THE PROBLEM OF SMALL SIZE FOR DIRECTIONAL HEARING....	2
II.	THE DESCRIPTION OF ORMIINE FLIES.....	5
A.	THE MECHANICAL ANALOGUE OF THE INTERTYMPANAL COUPLING.....	7
B.	MULTI DEGREE OF FREEDOM VIBRATION.....	10
C.	FREQUENCY RESPONSE FUNCTION.....	12
D.	THE EAR'S SENSITIVITY THE DIRECTION OF SOUND.....	15
III.	SENSOR DESIGN.....	17
A.	FABRICATED SENSOR CHIP (DESIGNED USING MEMSPRO).....	18
B.	EXPERIMENT SETUP.....	19
C.	MEASURED FREQUENCY RESPONSE (DEVICE 4 AND 6).....	22
D.	SIMULATED FREQUENCY RESPONSE (DEVICE 4 AND 6).....	24
IV.	THE MECHANICAL TO ELECTRICAL TRANSFORMATION (PSPICE).....	27
A.	IMPEDANCE ANOLOGY FOR DEVICE 4 (PERFORATED WINGS).....	29
B.	IMPEDANCE ANOLOGY FOR DEVICE 6 (SOLID WINGS).....	29
C.	PEAK HEIGHT, PEAK WIDTH AND QUALITY FACTOR.....	30
D.	TRANSIENT TIME OF RESPONSE.....	32
E.	ROCKING AND BENDING AMPLITUDE RATIO WITH INCIDENCE ANGLE OF SOUND.....	33
V.	CONCLUSION.....	35
VI.	RECOMMENDATIONS FOR FUTURE WORK.....	37
	LIST OF REFERENCES.....	39
	INITIAL DISTRIBUTION LIST.....	41

LIST OF FIGURES

Figure 1.	External auditory anatomy of <i>Ormia ochracea</i> . In ormiine flies, the tympanal ears are located between the first pair of legs and the base of the neck. The light scanning micrographs show a semilateral view of an intact fly (A), and (B) of a fly with the head removed to see the prosternal hearing organs. Co, prothoracic coax; N, neck; PTM, prosternal tympanal membranes; Pb, probasisternum; MSP, mesothoracic spiracle (Lakes Harlan and Heller 1992; Robert, Amoroso, and Hoy 1992).....	5
Figure 2.	Scanning electron micrographs of two closely related species of tachinid flies illustrating, in frontal view, the anatomical differences of the prosternal region. A. The tympanate fly <i>Ormia ochracea</i> . B. The atympanate fly <i>Myioppharus doryphorae</i> . PeS, proepisternal setae; PTM, prosternal tympanal membranes; PM, prosternal membranes; Pb, probasisternum; Pr, presternum; Co, prothoracic coax; N, neck; CSc, cervical sclerite. Notably, in the tympanate species (A) the Pb and the Pr are conspicuously larger, and the PTMs present a larger surface area and are thrown with radial corrugations. The small cuticular depressions at the distal ends of the Pr are the points of insertion of the sensory organs with the tympanal system. Scale 200 μm (Edgecomb et al. 1995; Robert et al. 1996a).	7
Figure 3.	The ears of <i>O. ochracea</i> and a mechanical model used to describe the directional sensitivity. The two tympana are the corrugated membranes that are mechanically connected through the intertympanal bridge, shown here with the numbers 1, 2, and 3. The central point (3) acts as a hinge.	8
Figure 4.	Schematized response of the intertympanal bridge.....	9
Figure 5.	The mechanical model includes equivalent stiffness, K_t and K_s equivalent viscous dashpots, C_t and C_s	11
Figure 6.	Free body diagram of a two Degree of Freedom system (see Taylor & Francis Group LLC, 2005).....	11
Figure 7.	Time delay between the ipsilateral and contralateral mechanical response, calculated from the difference phase spectrum from sound source at incident angle.....	13
Figure 8.	Phase difference and ratio of amplitude are independent of sound pressure.	16
Figure 9.	Layout of the 4 th generation chip. The Devices 4 and 6 are characterized in this work.	17
Figure 10.	Sensor is designed to achieve the desirable operating frequency.....	18
Figure 11.	The characteristics of both wings of each device. A. Device 4 (perforated wings). B. Device 6 (solid wings).	19
Figure 12.	The air gaps between the silicon substrate and the wings.	19

Figure 13.	The existing equipment used for measuring vibrational amplitudes. A. Rotating sound source. B. Sensor devices and microphone. C. Speaker for sound source with directional cone. D. Laser vibrometer.	20
Figure 14.	Rotating stage for the sound source.....	21
Figure 15.	Sensor and microphone.	21
Figure 16.	Speaker for sound source with directional cone.	22
Figure 17.	Laser vibrometer for measuring displacement amplitudes under sound excitation.	22
Figure 18.	The measured frequency response for Device 4 (perforated wings) and 6 (solid wings).....	23
Figure 19.	Deflection shapes of (a) rocking and (b) bending modes.	24
Figure 20.	The simulated frequency response for Device 4 (perforated wings) and 6 (solid wings).....	25
Figure 21.	Electrical equivalent circuit of the mechanical model of the fly's hearing system in Figure 5.	27
Figure 22.	Simulated frequency response at 45° using PSPICE.	30
Figure 23.	The peak width of rocking frequency.	31
Figure 24.	Transient time of response measured by PSPICE. A. Device 6 (solid wings). B. Device 4 (perforated wings).	32
Figure 25.	Directional sensitivity of the mechanical response from COMSOL.....	33

THIS PAGE INTENTIONALLY LEFT BLANK

LIST OF TABLES

Table 1.	The sensor dimension for both devices.....	18
Table 2.	Electrical-Mechanical equivalencies.....	27
Table 3.	Mechanical and electrical quantities for Device 4.....	29
Table 4.	Mechanical and electrical quantities for Device 6.....	29
Table 5.	The comparison of two devices in term of peak height width, and quality factor.....	31
Table 6.	Difference in the amplitude of the mechanical response between the tympanal pits for different angles of sound incidence.....	34

THIS PAGE INTENTIONALLY LEFT BLANK

ACKNOWLEDGMENTS

I would like to acknowledge The Government of Brunei Darussalam for supporting me to complete my thesis and research from the beginning and special thanks to my thesis Advisor, Professor Gamani Karunasiri and Co-Advisor Bruce Denardo for his continual guidance, time and effort for making this research possible.

I also would like to express my heartfelt gratitude to Professor Brett Borden for teaching me the transfer function and creamer function. Besides that, I am also deeply indebted to Lt Cdr Mike Touse for helping me out to get familiar with the laser vibrometer. My parents, in laws and families are deserved special credit for giving me moral support and motivation me through the course of my research works. Last but not least, thank you to God for answering my helps whenever I need your helps to complete my thesis and Master Degree.

Last but not least, thank you to Breen Dix for doing grammatical correction for me.

THIS PAGE INTENTIONALLY LEFT BLANK

I. INTRODUCTION

A. INTRODUCTION

The new design of generation 4th of directional microphone is designed to make an improvement from the previous efforts of understanding the sensitivity of directional hearing. Many small animals depend on the ability to localize the sound sources (Richard R. Fay and Arthur N. Popper, 1992). All animals having two tympanal ear (eardrums) to localize sound by processing interaural differences either in the time of arrival or level of the acoustic pressure. When the size of the animal is very small to relative to the sound wavelength, these interaural differences can be too small to permit accurate processing by the central nervous system to allow sound source localization. By suitable coupling of the motions of the tympana, it is possible for each to respond preferentially to sound from certain directions. This paper is to analysis of micromechanical device inspired by the coupled ears of the parasitoid fly, *Ormia ochracea*, and its usefulness as a has inspired a novel, approach to constructing small device and, directional sound receivers (Daniel Robert and Ronald R. Hoy, 1998). The objective of this directional microphone is to design to make an improvement from previous efforts (Antonios Dritsas, June 2008) to understand the sensitivity of this method of directional hearing.

This paper is a continuation development from the previous model, which is trying to improve the effect for acoustic directional sensing. The generation 4th of Silicon devices studied shows significant potential for enabling the development of novel sensors for sound and vibration and has focused on the fabrication of small design for sound. This experiment is to demonstrate the improvement in speech intelligibility in noise to achieve directional acoustic response and I have seen very good improvements in solid state in its performance in terms of quality factor and the results presented here will also help enable the future development of a good design for direction finding.

B. BACKGROUND

Some large insects creatures can use only sound amplitude pressure difference and arrival time difference for their directional hearing and others such as insects can make use of both amplitude and phase. In humans head (diameter ≈ 17 cm), the difference in the time of arrival at the two ears is approximately 0.5 ms. In insects the part of the body carrying the ears is about 10 to 50 times smaller than the human head, and large differences in sound pressure at the ears only exist at high frequencies. Most insects thus have great difficulty in determining the direction of sound incidence by measuring the difference in time when the sound waves reach both the left and right ears. Alternative ways without involving the pressure component of sound is by studying the Mechanical analogue of the tympanal system.

C. THE PROBLEM OF SMALL SIZE FOR DIRECTIONAL HEARING

Animals use two basic acoustics cues, interaural time and amplitude differences, for the directional binaural detection of a sound source. From the physical laws of sound propagation in air and the diffraction of sound around solid bodies, it is apparent that very small animals such as insects face limitations in their ability to extract detectable interaural time and amplitude acoustic cues from the incident sound field (Middlebrooks and Green, 1991). In theory, given the small body size of the ormiine flies and the very short interaural distance, the generation of reliable interaural acoustic cues seems highly problematic.

It is important to mention, in passing, that time and amplitude acoustic cues are not necessarily required to localize an incident sound. Monaural sound localization by means of spectral cues is possible in humans under certain circumstances. The processing of spectral information for directional hearing in insects has not been given much attention and can therefore not be excluded from consideration. As the speed of sound 344 m/s in air, an interaural distance of 1 cm will only generate an interaural time difference of the incident sound

wave (ITD) of about 30 μs . Such, and even shorter, time delays admittedly pose a severe challenge to the nervous system in its typical temporal range of operation on the order of a millisecond. The other basic cue, the interaural intensity differences, has operational size limits that are related to the wavelength of the incident sound and the size, shape, and density of the body or head carrying the ears. It is generally accepted from acoustical diffraction theory that a ratio of 1:10 between size and wavelength does not give rise to measurable diffractive effects (Morse and Ingard, 1968).

For example, a spherical body of 7 mm in diameter does not significantly diffract sounds below a frequency of 5 kHz (with a wavelength of 68 mm), and therefore very little or even no difference in interaural sound pressure occurs. It uses 5 kHz as an example because it is the dominant frequency of field crickets' calling song and therefore is salient to its acoustic parasitoid as well.

In theory, given the small body size of the ormiine flies (a few millimeters in breadth) and the very short interaural distance (1.68 mm total width for both tympanal membranes taken together), the generation of reliable (and physiologically relevant) interaural acoustic cues seems highly problematic. Practically, how does the fly acoustically localize her cricket host singing at 5 kHz? In the fly's case, the body size to wavelength ratio is about 1:130, thus precluding the effects of diffraction as the source of interaural intensity difference. An angle of incidence of 90 degree relative to the normal is the best case for sound localization, and sound will travel from one side to the other of the most lateral margins of the tympanal membranes (1.68 mm apart) in about 4.9 μs . In sensory organs is about 1.5 μs , given their separations of 520 μs . Actual measurements made with custom-made probe microphones confirm these theoretical arguments. At 5 kHz, the interaural intensity difference is too small to be measured, (<1dB) either across the fly's body or at the tympanal membranes. The maximal interaural time delay measured by two phase-calibrated probe microphones positioned directly in front of the tympanal membranes is 1.45 μs . [Robert, Amoroso, and Hoy, 1992].

THIS PAGE INTENTIONALLY LEFT BLANK

II. THE DESCRIPTION OF ORMIINE FLIES

The ears of ormiine flies are positioned on the ventral prothorax, above and anterior to the first pair of legs and just behind the head (Figure 1.A) (Lakes-Harlan and Heller 1992; Robert, Amoroso, and Hoy 1992). The general design feature of the ormiine hearing organs is consistent with the design of other insectan tympanal organs (Robert, Read, and Hoy 1994; Hoy and Robert 1996). A tympanal ear in insects essentially consists of three basic, major morphological components:

1. A localized thinning of the 'cuticle' to provide a tympanal membrane, which is formed by the apposition of a modified, thin exocuticle and a tracheal air sac.
2. An air chamber backing the tympanal membrane, which is formed by the associated tracheal air sac.
3. A mechanoreceptive sensory organ of the scolopidial type, which is in indirect contact with either the tympanal membrane or the modified tracheal system abutting it.

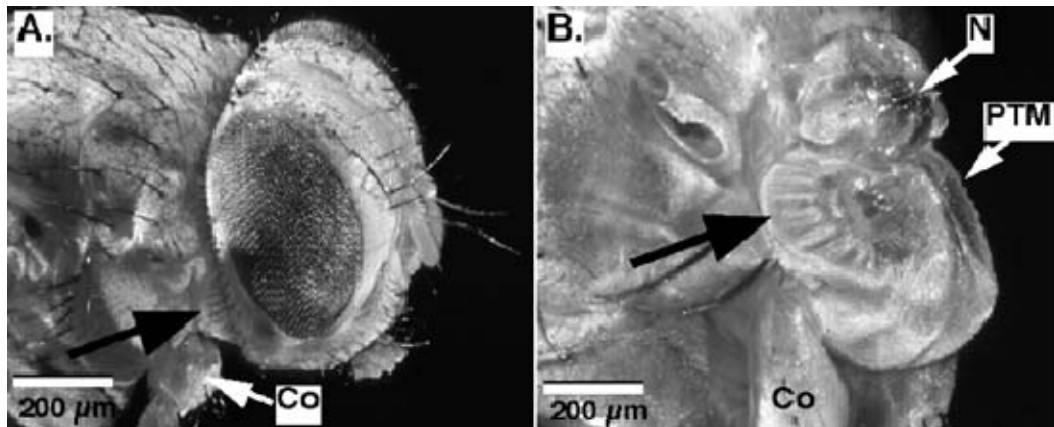


Figure 1. External auditory anatomy of *Ormia ochracea*. In ormiine flies, the tympanal ears are located between the first pair of legs and the base of the neck. The light scanning micrographs show a semilateral view of an intact fly (A), and (B) of a fly with the head removed to see the prosternal hearing organs. Co, prothoracic coxa; N, neck; PTM, prosternal tympanal membranes; Pb, probasisternum; MSP, mesothoracic spiracle (Lakes Harlan and Heller 1992; Robert, Amoroso, and Hoy 1992).

A series of eight morphological specializations that are particular to ormiines have been identified:

1. Enlargement of the prosternal membranes (PM), giving rise to thin prosternal tympanal membranes (PTM, see Figure 1.A), which present a relatively large surface area (compare Figure 2.A and 2.B).
2. Inflation of the ventral probasisternum (Pb) to provide structural support for the tympanal membranes.
3. Bilateral extensions of an unpaired sclerite associated with the tympanal membranes, the presternum (Pr), to which attach the sensory organs at the tympanal pits (TP). The biomechanical function of the presternum is a key to the process of directional hearing.
4. Enlargement of the prosternal air sac forming the acoustic chamber backing the tympanal membranes.
5. Location of the two scolopidial sensory organs in the unpartitioned prosternal air sac. A scolopidium is the elementary multicellular arrangement, including a mechanoreceptive neuron that is commonly used in insects for vibration reception.
6. Cuticular apodemes, establishing a stiff mechanical link between these sensory organs and the presternum.
7. Reduction in size of the prosternal cervical sclerites (CSc).
8. Structural reorganization of the internal endoskeleton of the prosternal region (Richard R. Fay and Arthur N Popper, 1998).

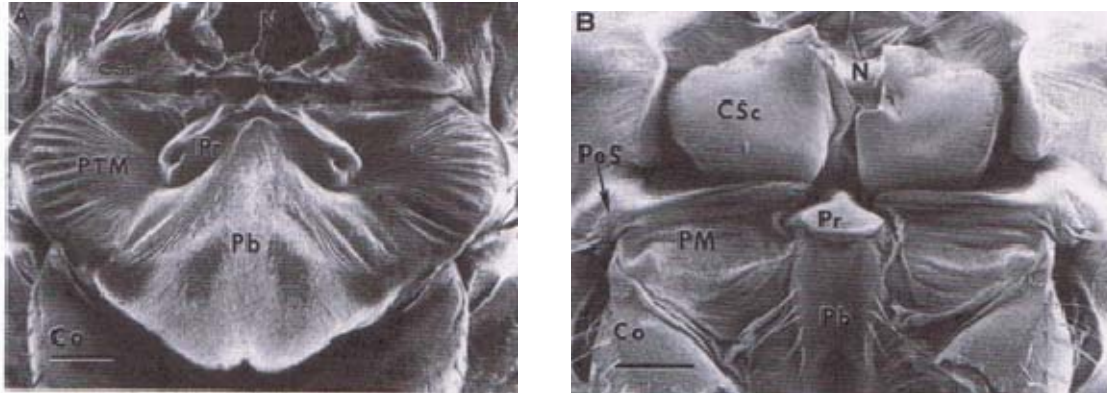


Figure 2. Scanning electron micrographs of two closely related species of tachinid flies illustrating, in frontal view, the anatomical differences of the prosternal region. A. The tympante fly *Ormia ochracea*. B. The atympante fly *Myioppharus doryphorae*. PeS, proepisternal setae; PTM, prosternal tympanal membranes; PM, prosternal membranes; Pb, probasisternum; Pr, presternum; Co, prothoracic coxa; N, neck; CSc, cervical sclerite. Notably, in the tympante species (A) the Pb and the Pr are conspicuously larger, and the PTMs present a larger surface area and are thrown with radial corrugations. The small cuticular depressions at the distal ends of the Pr are the points of insertion of the sensory organs with the tympanal system. Scale 200 μm (Edgecomb et al. 1995; Robert et al. 1996a).

A. THE MECHANICAL ANALOGUE OF THE INTERTYMPANAL COUPLING

Analysis of the deflection shapes of the tympanal membranes, and more particularly of the intertympanal bridge, indicates that the two ears, join at the pivot point. The incident pressure of sound produces deflection in two sides of the wing shaped tympana two deflections of wing, which are almost in phase and with the same amplitude. However, as shown in Figure 3, the intertympanal bridge undergoes an asymmetrical displacement about its center, much like a flexible seesaw rocking back and forth about its pivot point.

The intertympanal bridge that links the tympanal membranes is a key feature of the auditory mechanics of the ormiine ears. The ability of the intertympanal bridge to rock back and forth in a flexible manner is what can drive

both membranes with such phase and amplitude differences. The ability of the incident sound pressures to drive this tympanal system depends on the relative phase of the pressures acting on the tympana. In the same way, a seesaw is put out of static equilibrium by two weights of equal mass applied at different times on each of its ends; these forces (pressures) result in the rocking motion. As one arm of the bridge is deflected downward, the other arm will move upward due to the stiffness of the bridge (Figure 3).

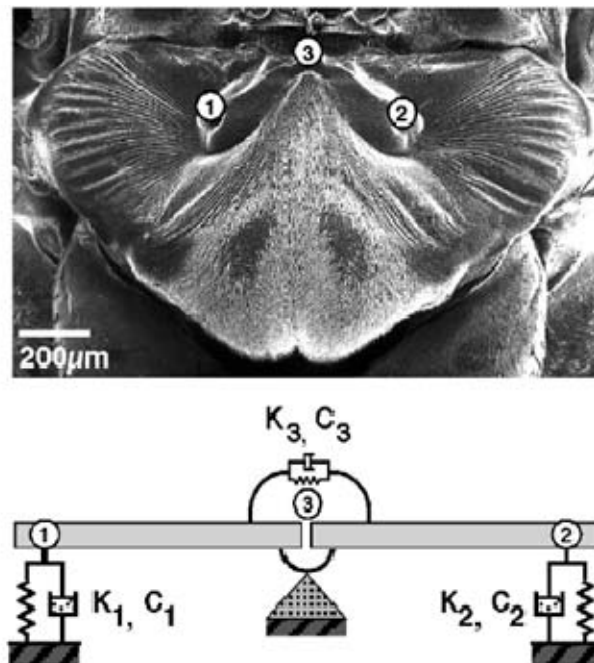


Figure 3. The ears of *O. ochracea* and a mechanical model used to describe the directional sensitivity. The two tympana are the corrugated membranes that are mechanically connected through the intertympanal bridge, shown here with the numbers 1, 2, and 3. The central point (3) acts as a hinge.

A more complete analysis of this system shows that the behavior of this mechanical system with two degrees of freedom can be explained by the interaction of two basic modes of vibration (one rotational, one translational).

The relative contributions of these modes at different driving frequencies depend on the difference or sum of the forces acting on the system and on its resonant properties (see Miles, Robert, and Hoy 1995; Robert, Miles, and Hoy 1996b).

This morphological and biomechanical evidence led to the development of a simple mechanical analogue, the mathematical formulation of which is presented in Miles, Robert, and Hoy (1995). In this model, the flexible intertympanal bridge is represented by two rigid bars connected medially by a torsional spring, and dash pot. Both extremities of the bridge are connected to a spring and a dash pot that represent the stiffness and damping characteristics of the auditory sensory organs attached to the tympanal pits.

The deflection shapes computed from laser vibrometer and COMSOL illustrate the unusual rocking and transitional motions of the intertympanal bridge. The resulting ipsilateral and contralateral motion amplitudes can be visualized in the sketch (Figure 4). Unfortunately, this representation does not illustrate the phase delay introduced by this floppy connection.

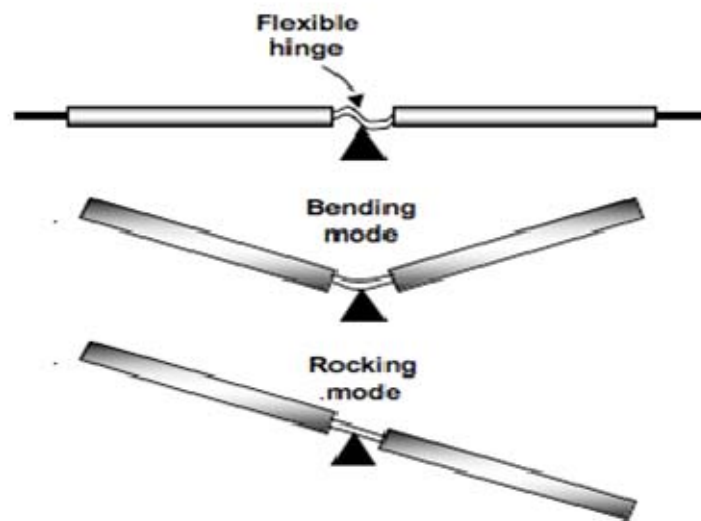


Figure 4. Schematized response of the intertympanal bridge.

However, the present evidence does not formally exclude that an alternative mechanism could account for, or contribute to, the observed tympanal dynamics. Indeed, it is still possible that the air space behind both tympanal membranes could have a sufficient stiffness to act as a resonator and thus provide the basis for a directional response, as is the case for the acoustically coupled ears of pressure difference receivers as in frogs and lizards. In a pressure difference system, the volume of the air chamber backing the tympana is crucial for the directionality to be determined by the mechanical response of the mechanical response of the tympana (see B. Hedwig, 2005).

B. MULTI DEGREE OF FREEDOM VIBRATION

In this section, a review of deterministic vibration is provided. These results are used in the next section, where the forcing is taken to be a random process. The equations of motion can be written as:

$$[m]\{\ddot{x}(t)\} + [c]\{\dot{x}(t)\} + [k]\{x(t)\} = \{F(t)\} \quad (1.1)$$

where the matrices $[m]$, $[c]$ and $[k]$ are of dimension $N \times N$, and the response $\{x(t)\}$ and force $\{F(t)\}$ vectors are dimension $N \times 1$.

This concept will be introduced primarily by working through the solution of a two degree of freedom system. All these ideas transfer to large systems, but with the two degree of freedom models, they can be demonstrated without complications of the major algebraic and numerical demands made by the larger systems.

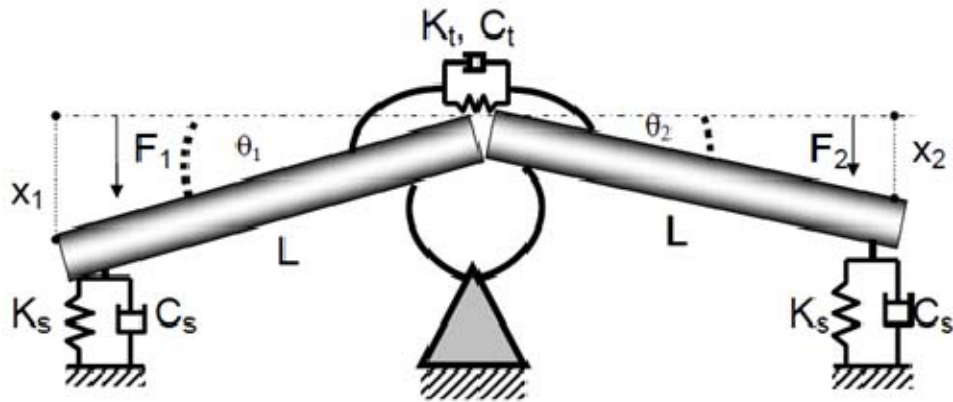


Figure 5. The mechanical model includes equivalent stiffness, K_t and K_s equivalent viscous dashpots, C_t and C_s .

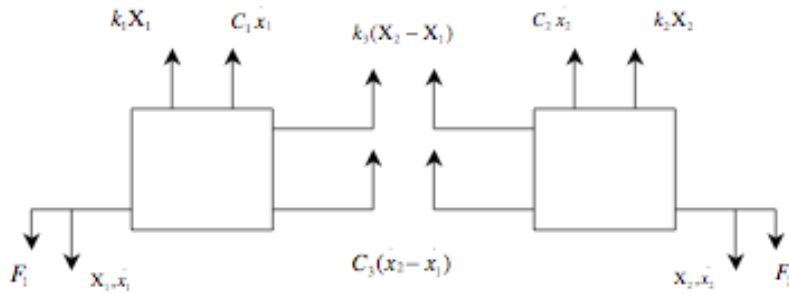


Figure 6. Free body diagram of a two Degree of Freedom system (see Taylor & Francis Group LLC, 2005).

From the diagram on Figure 5 and 6, motion can be derived using the coupled equation of motion using either Newton's Second Law of motion applied to a free body diagram for each mass or by Lagrange's equation. In either case, equations reduce to governing equations to be:

$$m \ddot{x}_1(t) + (c_1 + c_3) \dot{x}_1(t) + c_3 \dot{x}_2(t) + (k_1 + k_2) x_1(t) + k_3 x_2(t) = F_1(t) \quad (1.2)$$

$$m \ddot{x}_2(t) + (c_2 + c_3) \dot{x}_2(t) + c_3 \dot{x}_1(t) + k_3 x_1(t) + (k_2 + k_3) x_2(t) = F_2(t) \quad (1.3)$$

In matrix form turn to be:

$$\begin{bmatrix} m_1 & 0 \\ 0 & m_2 \end{bmatrix} \begin{Bmatrix} \ddot{x}_1(t) \\ \ddot{x}_2(t) \end{Bmatrix} + \begin{bmatrix} c_1 + c_3 & c_3 \\ c_3 & c_2 + c_3 \end{bmatrix} \begin{Bmatrix} \dot{x}_1(t) \\ \dot{x}_2(t) \end{Bmatrix} + \begin{bmatrix} k_1 + k_3 & k_3 \\ k_3 & k_2 + k_3 \end{bmatrix} \begin{Bmatrix} x_1(t) \\ x_2(t) \end{Bmatrix} = \begin{Bmatrix} F_1(t) \\ F_2(t) \end{Bmatrix} \quad (1.4)$$

For this case, the three parameters of the mass, damping, and stiffness are given by

$$[m] = \begin{bmatrix} m_1 & 0 \\ 0 & m_2 \end{bmatrix}, \quad [c] = \begin{bmatrix} c_1 + c_3 & c_3 \\ c_3 & c_2 + c_3 \end{bmatrix}, \quad [k] = \begin{bmatrix} k_1 + k_3 & k_3 \\ k_3 & k_2 + k_3 \end{bmatrix} \quad (1.5)$$

C. FREQUENCY RESPONSE FUNCTION

Begin by taking the Fourier transform of the equations of motion, obtaining

$$(-\omega^2 [m] + i\omega [c] + [k]) \{X(\omega)\} = \{F(\omega)\} \quad (1.6)$$

where $X(\omega)$ and $F(\omega)$ are Fourier transforms of $x(t)$ and $F(t)$. The matrix $(-\omega^2 [m] + i\omega [c] + [k])$ is denoted as $[Z(\omega)]$. Then

$$\{X(\omega)\} = [Z(\omega)]^{-1} \{F(\omega)\} \quad (1.7)$$

The matrix $[Z(\omega)]^{-1}$ is identical to the frequency response matrix denoted as $[H(\omega)]$:

$$\{X(\omega)\} = [H(\omega)]\{F(\omega)\} \quad (1.8)$$

The transfer functions are given by $H_{f1p}(\omega) = se^{i\omega\tau/2}$ and $H_{f2p}(\omega) = se^{-i\omega\tau/2}$, where τ is the time for the incident sound to travel between the points where the forces act as given above and s is the surface area of each tympanal membrane as shown below.

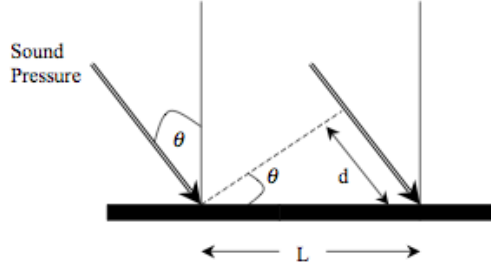


Figure 7. Time delay between the ipsilateral and contralateral mechanical response, calculated from the difference phase spectrum from sound source at incident angle.

The distance of d is the distance sound travel with respects to the angle θ and c (speed of sound). The time delay of τ can be determined as:

$$\tau = \frac{d}{c} = \frac{L \sin \theta}{c} \quad (1.9)$$

The transfer functions between the responses and the pressure at the pivot may be found using Cramer's rules, a method to solve systems equations using determinants. Starting with equation below:

$$-\omega^2 \begin{bmatrix} m_1 & 0 \\ 0 & m_2 \end{bmatrix} \begin{bmatrix} x_1 \\ x_2 \end{bmatrix} + i\omega \begin{bmatrix} c_1 + c_3 & c_3 \\ c_3 & c_2 + c_3 \end{bmatrix} \begin{bmatrix} x_1 \\ x_2 \end{bmatrix} + \begin{bmatrix} k_1 + k_3 & k_3 \\ k_3 & k_2 + k_3 \end{bmatrix} \begin{bmatrix} x_1 \\ x_2 \end{bmatrix} = \begin{bmatrix} F_1 \\ F_2 \end{bmatrix} \quad (1.10)$$

$$\begin{bmatrix} -\omega^2 m_1 - i\omega(c_1 + c_3) + k_1 + k_3 & -i\omega c_3 + k_3 \\ -i\omega c_3 + k_3 & -\omega^2 m_2 - i\omega(c_2 + c_3) + k_2 + k_3 \end{bmatrix} \begin{bmatrix} x_1 \\ x_2 \end{bmatrix} = \begin{bmatrix} F_1 \\ F_2 \end{bmatrix} \quad (1.11)$$

By Cramer's rules method, the transfer function between $H_{x_1p}(\omega)$ and $H_{x_2p}(\omega)$ the responses and the pressure at the pivot are shown below:

$$H_{x_1p}(\omega) = \frac{\det \begin{bmatrix} F_1 & -i\omega c_3 + k_3 \\ F_2 & -\omega^2 m_2 - i\omega(c_2 + c_3) + k_2 + k_3 \end{bmatrix}}{\det \begin{bmatrix} -\omega^2 m_1 - i\omega(c_1 + c_3) + k_1 + k_3 & -i\omega c_3 + k_3 \\ -i\omega c_3 + k_3 & -\omega^2 m_2 - i\omega(c_2 + c_3) + k_2 + k_3 \end{bmatrix}} \quad (1.12)$$

$$H_{x_1p}(\omega) = \frac{s(k_3 + i\omega c_3) \times (e^{i\omega\tau/2} - e^{-i\omega\tau/2}) + s(k + i\omega c - m\omega^2)e^{i\omega\tau/2}}{(k + i\omega c + k_3 + i\omega c_3 - m\omega^2)^2 - (k_3 + i\omega c_3)^2} \quad (1.13)$$

$$H_{x_2p}(\omega) = \frac{\det \begin{bmatrix} -\omega^2 m_1 - i\omega(c_1 + c_3) + k_1 + k_3 & F_1 \\ -i\omega c_3 + k_3 & F_2 \end{bmatrix}}{\det \begin{bmatrix} -\omega^2 m_1 - i\omega(c_1 + c_3) + k_1 + k_3 & -i\omega c_3 + k_3 \\ -i\omega c_3 + k_3 & -\omega^2 m_2 - i\omega(c_2 + c_3) + k_2 + k_3 \end{bmatrix}} \quad (1.14)$$

$$H_{x_2p}(\omega) = \frac{s(k_3 + i\omega c_3) \times (e^{-i\omega\tau/2} - e^{i\omega\tau/2}) + s(k + i\omega c - m\omega^2)e^{-i\omega\tau/2}}{(k + i\omega c + k_3 + i\omega c_3 - m\omega^2)^2 - (k_3 + i\omega c_3)^2} \quad (1.15)$$

where,

$$\text{Rocking frequency, } \omega_r = \sqrt{\frac{k}{m}} \quad (1.16)$$

$$\text{Bending frequency, } \omega_t = \sqrt{\frac{(k + 2k_3)}{m}} \quad (1.17)$$

$$\xi_r = \frac{c}{2\omega_r m}, \quad \xi_t = \frac{(c + 2c_3)}{2\omega_t m} \quad (1.18)$$

To simplify the notation, let $H_{f_1p}(\omega)$ and $H_{f_2p}(\omega)$ denote the transfer functions as a function of the frequency, ω , in radians/s of the ipsilateral and contralateral force $f_1(t)$, and $f_2(t)$, relative to the acoustic pressure at the microphone location, $p(t)$. The solutions of modes for the transfer function in Equation.1.12 and 1.14 are given by:

$$H_{x_1p}(\omega) = \frac{(H_{f_1p}(\omega) - H_{f_2p}(\omega)) / m}{\omega_r^2 - \omega^2 + 4\omega_r \xi_r i\omega} + \frac{(H_{f_1p}(\omega) + H_{f_2p}(\omega)) / m}{\omega_t^2 - \omega^2 + 4\omega_t \xi_t i\omega} \quad (1.19)$$

$$H_{x_2p}(\omega) = \frac{(H_{f_1p}(\omega) + H_{f_2p}(\omega)) / m}{\omega_t^2 - \omega^2 + 4\omega_t \xi_t i\omega} - \frac{(H_{f_1p}(\omega) - H_{f_2p}(\omega)) / m}{\omega_r^2 - \omega^2 + 4\omega_r \xi_r i\omega} \quad (1.20)$$

where $H_{x_1p}(\omega)$ and $H_{x_2p}(\omega)$ are the transfer functions between the responses of the ends of the tympanal bridge, $x_1(t)$ and $x_2(t)$, relative to the pressure at the pivot point, $p(t)$ (see Miles, Robert, and Hoy 1995).

D. THE EAR'S SENSITIVITY TO THE DIRECTION OF SOUND

The expression of the two oscillation are described as in Equation 1.20 to 1.22 which is explained at Figure 5 and 8 for two Eigen modes (G. Karunasiri, 2008). The displacements of the two sides can be expressed as:

$$A_r = \frac{Ps}{m} \left[\frac{\sin\left(\frac{\omega d \sin \theta}{2V_s}\right)}{\sqrt{(\omega_r^2 - \omega^2)^2 + (\gamma_r \omega)^2}} \right], \quad A_b = \frac{Ps}{m} \left[\frac{\sin\left(\frac{\omega d \sin \theta}{2V_s}\right)}{\sqrt{(\omega_b^2 - \omega^2)^2 + (\gamma_b \omega)^2}} \right] \quad (1.21)$$

$$A_1^2 = A_b^2 + A_r^2 + 2A_bA_r \sin(\phi_b - \phi_r), A_2^2 = A_b^2 + A_r^2 - 2A_bA_r \sin(\phi_b - \phi_r) \quad (1.22)$$

$$x_1 = A_1 \sin(\omega t + \phi_1), x_2 = A_2 \sin(\omega t + \phi_2) \quad (1.23)$$

where A_1 and A_2 are the amplitudes of ipsilateral and contralateral and ϕ_1 and ϕ_2 are the corresponding phases (Figure 8). The sound direction can be determined by looking at the amplitude and the phase difference between ipsilateral and contralateral.

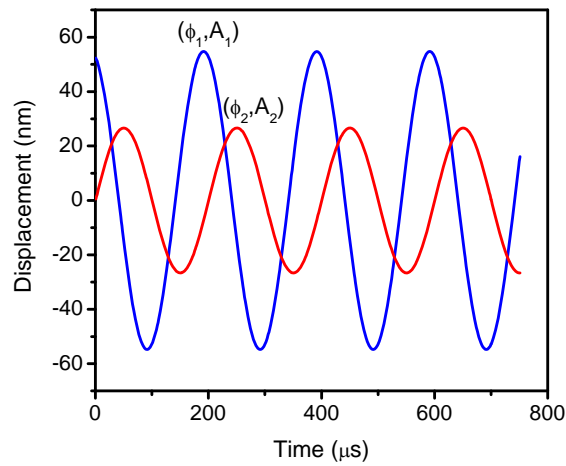


Figure 8. Phase difference and ratio of amplitude are independent of sound pressure.

III. SENSOR DESIGN

The 4th generation sensor chip contains 12 different sensors as shown in Figure 9. The chip was fabricated using SOIMUMPs process available through the MEMSCAP foundry service (SOIMUMPs Design Handbook, Rev. 4.0).

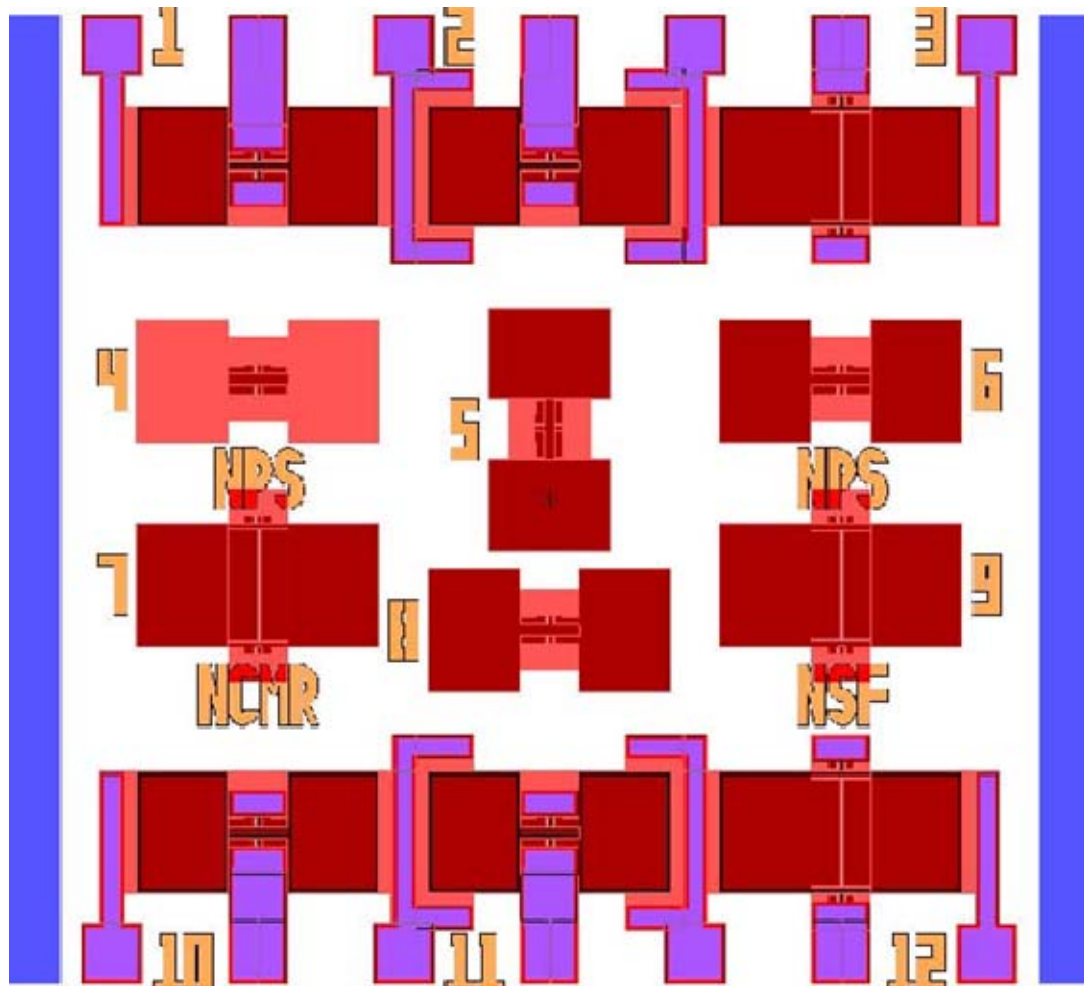


Figure 9. Layout of the 4th generation chip. The Devices 4 and 6 are characterized in this work.

In the following, details of the Devices 4 and 6 in the layout shown in Figure 10 are given since they are extensively characterized in the work. Dimensionally they are identical except the Device 4 the wings are perforated with square holes having of $2 \times 2 \mu\text{m}^2$ area. The Table 1 gives the dimensions of the structure.

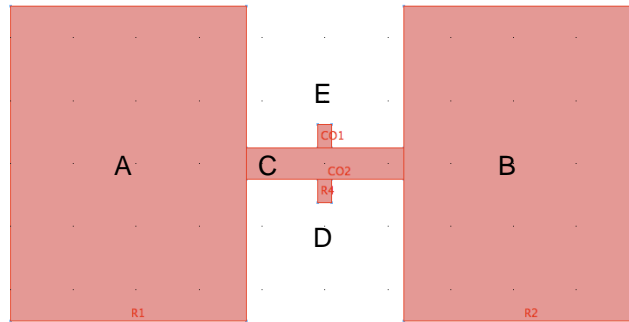


Figure 10. Sensor is designed to achieve the desirable operating frequency.

	A and B	C	D and E
Dimension	1 mm x 0.75 mm	0.080 mm x 0.5 mm	0.045 mm x 0.075 mm

Table 1. The sensor dimension for both devices.

A. FABRICATED SENSOR CHIP (DESIGNED USING MEMSPRO)

Figure 11 shows the expanded view of the two devices. The substrate under the devices was trenced during the processing to reduce squeezed film damping as depicted in Figure 12.

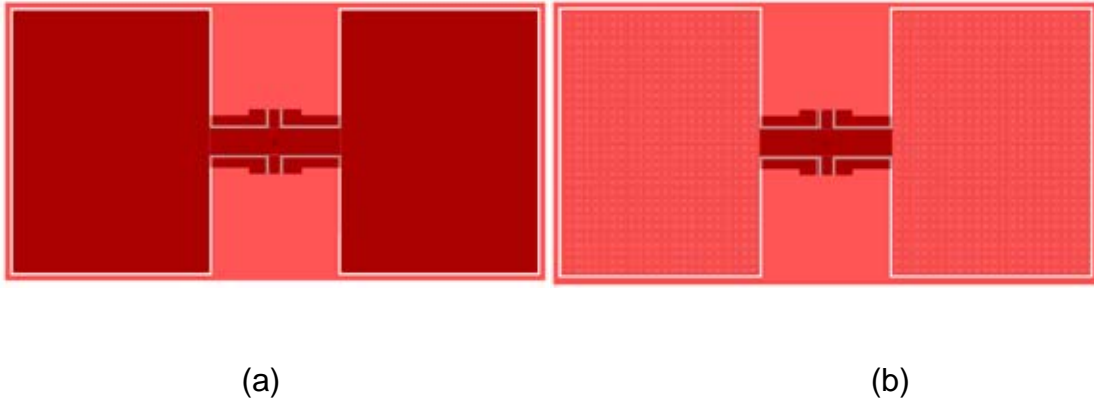


Figure 11. The characteristics of both wings of each device. A. Device 4 (perforated wings). B. Device 6 (solid wings).

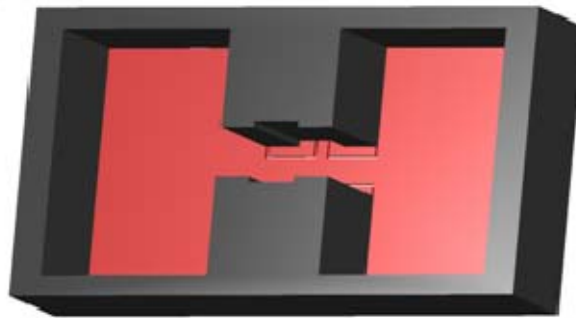


Figure 12. The air gaps between the silicon substrate and the wings.

One of the main goals of the research is the probe the effects of holes on the device 4 on the dynamics of the sensor response. In particular, the coupling of sound and enhanced damping due to possible airflow through the holes.

B. EXPERIMENT SETUP

Figure 13 shows a picture of the laboratory setup used to measure the vibrational amplitudes of the sensors under sound excitation. The experiment setup consists of the reference microphone, speaker on a rotating boom, laser

vibrometer, and devices. The reference microphone was placed close to the sensor chip to measure the sound pressure. It is a Bruel & Kjaer Pressure field $\frac{1}{8}$ " microphone type 4138. It has a relatively flat response curve from 20 Hz to 20 kHz with 0.939 mV/Pa sensitivity.

The sound source was Selenium loudspeaker type DH200E attached to the internal signal generator in the VibSoft software. The software allows the generation of pure tones as well as chirp sound with different amplitude and frequency. Incident sound wave angle was adjusted manually by adjusting the speaker position. The laser vibrometer was a Polytec single point vibrometer model OFV 302, with a model OFV 2600 controller. Its purpose was to measure the displacement of the wings, to a resolution in the sub nanometer range. (Antonios Dritsas, thesis paper, June 2008).

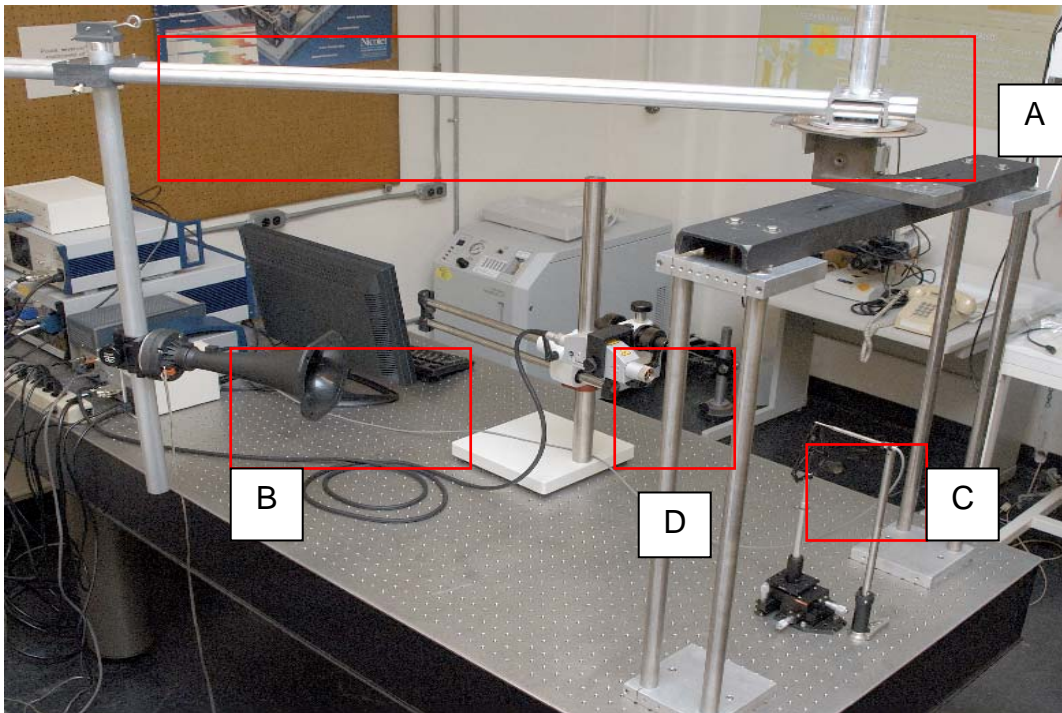


Figure 13. The existing equipment used for measuring vibrational amplitudes. A. Rotating sound source. B. Sensor devices and microphone. C. Speaker for sound source with directional cone. D. Laser vibrometer.

The sound source attached to the rotating stage in Figure 14 is used to measure the response at a discrete set of angles.



Figure 14. Rotating stage for the sound source.

The location of the reference microphone relative to the sensor chip is shown in Figure 15. The microphone is connected to the reference input of the laser vibrometer.

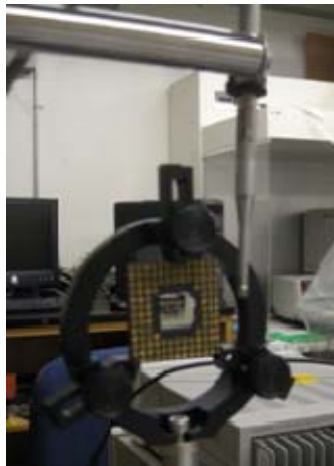


Figure 15. Sensor and microphone.

The speaker (see Figure 16) used as the sound source has a relatively flat response in the 1–2 kHz frequency range consists of a cone to direct the sound towards the sensor.



Figure 16. Speaker for sound source with directional cone.

The laser vibrometer shown in Figure 17 is to measure the vibration amplitudes of the wings in response to incident sound at different angles. The typical displacements of the wings are in the tens of nanometers.

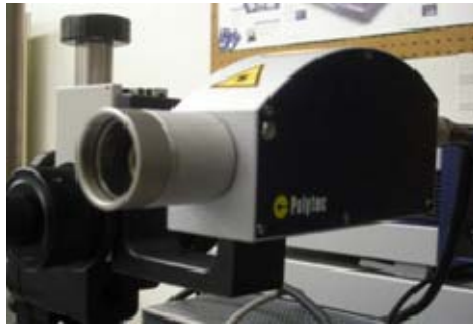


Figure 17. Laser vibrometer for measuring displacement amplitudes under sound excitation.

C. MEASURED FREQUENCY RESPONSE (DEVICE 4 AND 6)

The deflection amplitudes computed from the laser vibrometer measurements illustrate the expected rocking and bending motions of the wings of the sensors. The measured rocking and bending motion amplitudes as a function of frequency for the two devices at 45° are shown in the Figure 18. The measured amplitude at the bending mode is about $10 \mu\text{m}$ per 1 Pa of sound

pressure. The amplitudes at the rocking motion were relatively small since it depends on the arrival time difference between the two wings, which is order of a few microseconds.

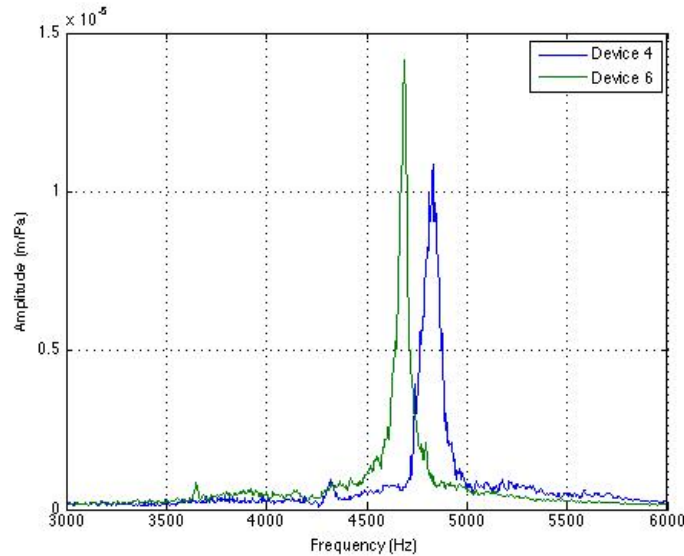


Figure 18. The measured frequency response for Device 4 (perforated wings) and 6 (solid wings).

The sound intensity is set by applying 0.1 Volt to the controller, which is connected to an amplifier for driving the speaker. The amplifier generates an output voltage depending on the gain used to drive the sound source. The signal from the reference microphone was converted to pressure using its conversion factor of 0.939 V/Pa. The measured rocking frequency of the Device 4 and Device 6 were approximately at 4385 Hz and 3680 Hz, respectively while the bending mode are found to be around 4850 Hz and 4620 Hz as shown in Figure 18. The two devices show different resonant frequencies as well as peak amplitude. The Device 4 (perforated wings) shows slightly smaller amplitude of deflection for both the rocking and bending modes compared to that of the Device 6 (solid wings) as depicted in Figure 20.

In experiment, the response of the sensors was also investigated by random noise analysis. In this analysis, the stimulus was a band limited random noise burst (500 to 8000 Hz bandwidth) delivered at 45° of incidence angle. The mechanical responses of the ipsilateral and contralateral are measured by positioning the beam of the laser vibrometer on the locations indicated in Figure 3. The ipsilateral side found to vibrate in the sound field with slightly higher amplitude than the contralateral side.

D. SIMULATED FREQUENCY RESPONSE (DEVICE 4 AND 6)

In order to compare the measured frequency responses with the designed values, a finite element analysis was carried out using COMSOL. Figure 19 shows the simulated rocking and bending motions of the sensor with solid wings.

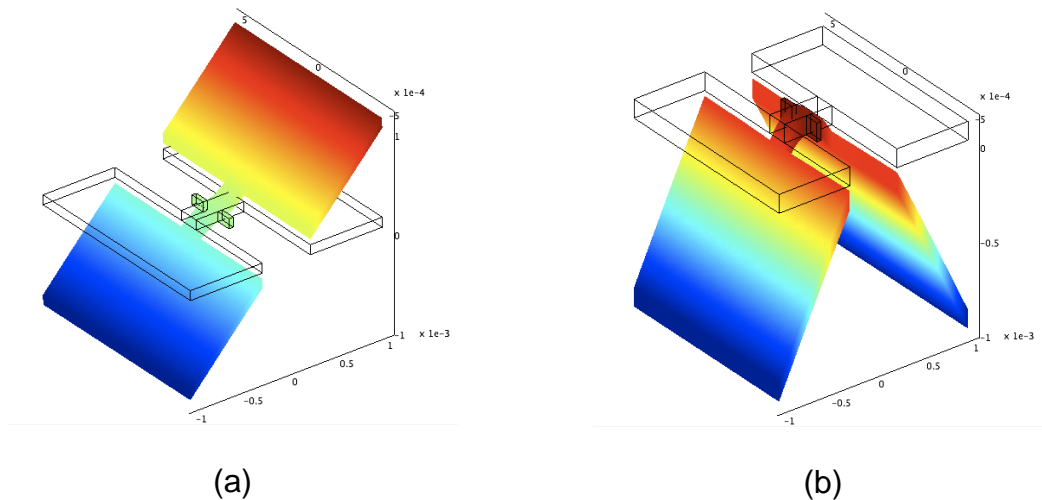


Figure 19. Deflection shapes of (a) rocking and (b) bending modes.

The simulated frequency responses of the two devices show different peak amplitudes and frequencies. Device 4 (perforated wings) shows smaller deflection than Device 6 (solid wings) in both modes as shown in Figure 20. The simulated frequency responses are in good agreement with the measured data shown in Figure 18.

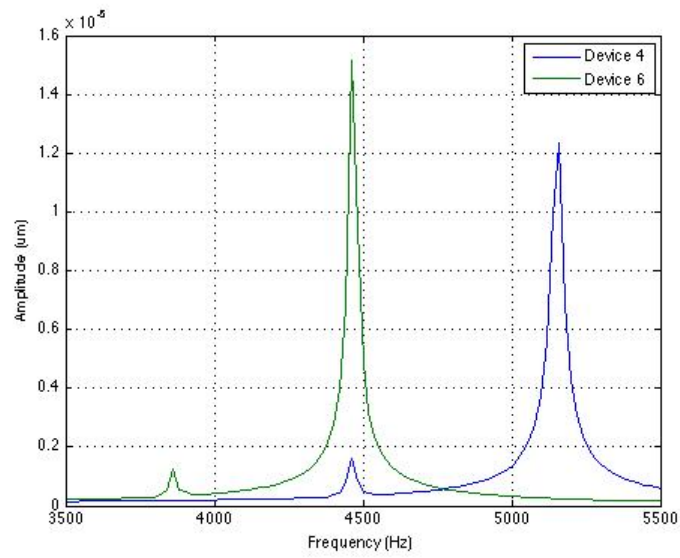


Figure 20. The simulated frequency response for Device 4 (perforated wings) and 6 (solid wings).

THIS PAGE INTENTIONALLY LEFT BLANK

IV. THE MECHANICAL TO ELECTRICAL TRANSFORMATION (PSPICE)

In order to determine the speed of operation of the sensors, the transient response of them were analyzed using SPICE circuit simulator based on electrical and mechanical equivalents. The following briefly discusses the analogies between electrical and mechanical components. Table 2 lists the correspondence between mechanical and electrical quantities.

MECHANICAL QUANTITY	ELECTRICAL QUANTITY
Force, F	Electromotive force, V
Velocity, u	Current, I
Displacement, $x = \int u dt$	Charge, $q = \int I dt$
Mass, M	Inductance, L
Mechanical Resistance, R_m	Resistance, R
Stiffness, k_m	Capacitance, $1/C$

Table 2. Electrical-Mechanical equivalencies.

Based on the equivalent quantities shown in Table 2, the electrical equivalent circuit of the mechanical model of the fly's hearing system in Figure 5 can be constructed as shown in Figure 21.

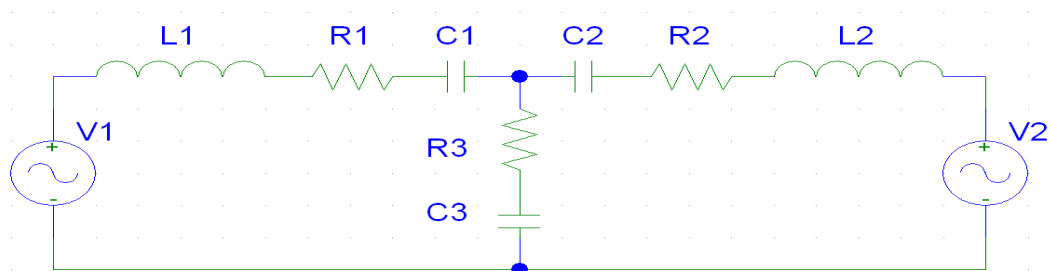


Figure 21. Electrical equivalent circuit of the mechanical model of the fly's hearing system in Figure 5.

The differential equations of motion for the mechanical system and the electrical circuit have the same form as shown by Equations 1.24 - 1.27.

$$M \ddot{x}_1 + (C_1 + C_3) \dot{x}_1 + C_3 \dot{x}_2 + (k_1 + k_3)x_1 + k_3 x_2 = F_1 \quad (1.24)$$

$$L \frac{d^2 q_1}{dt^2} + (R_1 + R_3) \frac{dq_1}{dt} + R_3 \frac{dq_2}{dt} I_2 + \left(\frac{1}{C_1} + \frac{1}{C_3} \right) q_1 + \frac{1}{C_3} q_2 = V_1 \quad (1.25)$$

$$M \ddot{x}_2 + C_3 \dot{x}_1 + (C_2 + C_3) \dot{x}_2 + k_3 x_1 + (k_2 + k_3)x_2 = F_2 \quad (1.26)$$

$$L \frac{d^2 q_2}{dt^2} + R_3 \frac{dq_1}{dt} + (R_2 + R_3) \frac{dq_2}{dt} + \frac{1}{C_3} q_1 + \left(\frac{1}{C_2} + \frac{1}{C_3} \right) q_2 = V_2 \quad (1.27)$$

The analogy is very useful because the equivalent electrical circuit can be readily solved using PSPICE. The parameter of the electrical circuit was obtained from the measured frequency responses of the two sensors given in Figure 21. The mass of each wing was estimated based on the dimension and density of Si and the mechanical resistance was estimated using the peak widths and Tables 3 and 4 list the parameters for the sensors with perforated and solid wings, respectively.

A. IMPEDANCE ANOLOGY FOR DEVICE 4 (PERFORATED WINGS)

Mechanical Quantity		Electrical Quantity		Remarks
Mechanical Resistance	R _{m1} and R _{m2} (3×10^{-6} kg/s)	Resistor	R ₁ and R ₂ (3×10^{-6} Ω)	R _{m1} and R _{m2} = R ₁ and R ₂
	R _{m3} (5.2×10^{-6} kg/s)		R ₃ (5.2×10^{-6} Ω)	R _{m3} = R ₃
Mass	M ₁ and M ₂ (4.66×10^{-9} kg/s)	Inductor	L ₁ and L ₂ (4.66×10^{-9} Ω)	M ₁ and M ₂ = L ₁ and L ₂
Stiffness	k ₁ and k ₂ (3.71 N/m)	Capacitance	C ₁ and C ₂ (0.27 F)	k ₁ and k ₂ = $\frac{1}{C_1}$ and $\frac{1}{C_2}$
	k ₃ (0.685 N/m)		C ₃ (1.46 F)	k ₃ = $\frac{1}{C_3}$

Table 3. Mechanical and electrical quantities for Device 4.

B. IMPEDANCE ANOLOGY FOR DEVICE 6 (SOLID WINGS)

Mechanical Quantity		Electrical Quantity		Remarks
Mechanical Resistance	R _{m1} and R _{m2} (2.93×10^{-6} kg/s)	Resistor	R ₁ and R ₂ (2.93×10^{-6} Ω)	R _{m1} and R _{m2} = R ₁ and R ₂
	R _{m3} (4.2×10^{-6} kg/s)		R ₃ (4.2×10^{-6} Ω)	R _{m3} = R ₃
Mass	M ₁ and M ₂ (4.66×10^{-9} kg/s)	Inductor	L ₁ and L ₂ (4.66×10^{-9} Ω)	M ₁ and M ₂ = L ₁ and L ₂
Stiffness	k ₁ and k ₂ (2.632 N/m)	Capacitance	C ₁ and C ₂ (0.38 F)	k ₁ and k ₂ = $\frac{1}{C_1}$ and $\frac{1}{C_2}$
	k ₃ (0.526 N/m)		C ₃ (1.9 F)	k ₃ = $\frac{1}{C_3}$

Table 4. Mechanical and electrical quantities for Device 6.

This graph in Figure 22 shows the calculated amplitudes using PSPICE based on the circuit described in Figure 21. The amplitudes were estimated based on the charge accumulated on the capacitors. For the Device 4, the rocking amplitude is about $0.76 \mu\text{m}$ ($C_1V = 0.27\text{F} \times 2.8\mu\text{V}$) and $12.41 \mu\text{m}$ for the bending frequency, ($C_3V = 1.46\text{F} \times 8.5\mu\text{V}$). The corresponding values for the Device 6 were found to be about $1.06 \mu\text{m}$ for rocking frequency and $10.5 \mu\text{m}$ for bending frequency.

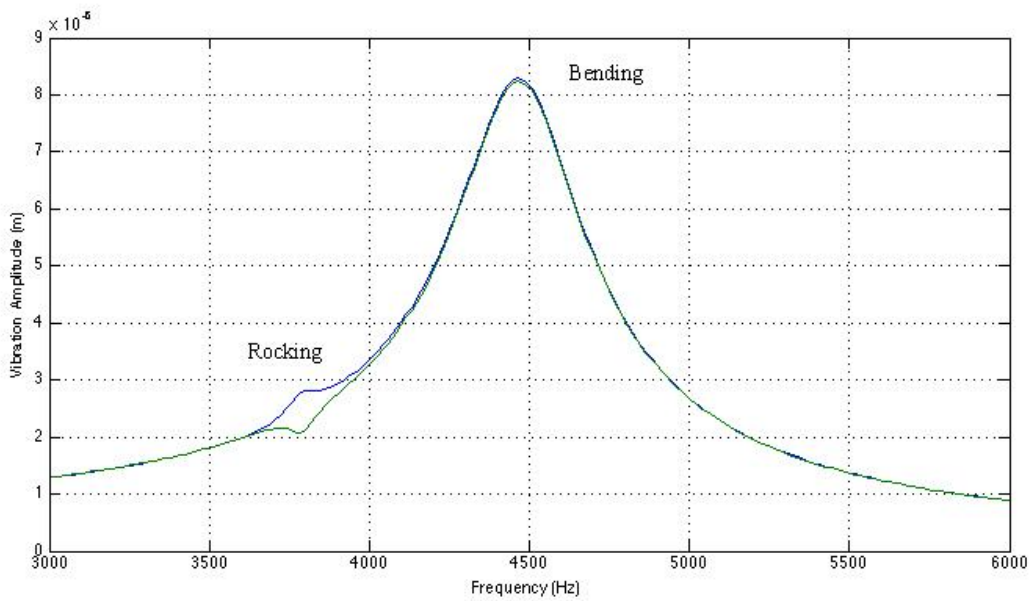


Figure 22. Simulated frequency response at 45° using PSPICE.

C. PEAK HEIGHT, PEAK WIDTH AND QUALITY FACTOR

The COMSOL simulated and measured amplitudes, peak widths and quality factors (Q) for the Devices 4 (perforated wings) and 6 (solid wings) are shown in Table 5. The width of the peak is defined as the distance between the two half-power points at $\pm 3\text{dB}$ frequencies as in Figure 23. The distance between half power points is referred to as the bandwidth:

$$\text{Peak width} = f_{+3\text{dB}} - f_{-3\text{dB}} \quad (1.28)$$

The quality factor is a term used to describe the sharpness of the peak as it defines by:

$$\text{Quality Factor, } Q = \frac{f_o}{f_{+3\text{dB}} - f_{-3\text{dB}}} \quad (1.29)$$

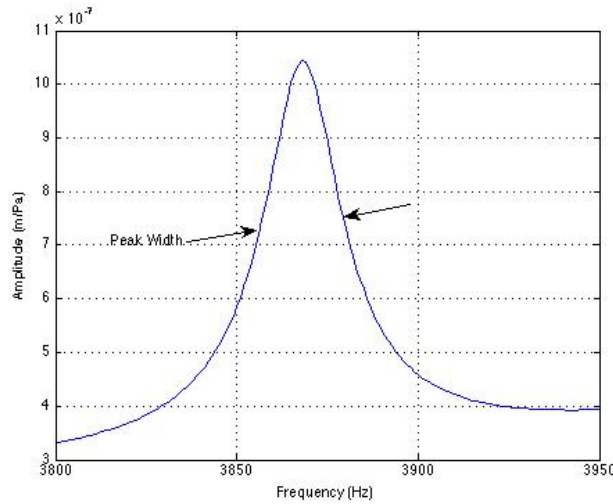


Figure 23. The peak width of rocking frequency.

	COMSOL		LASER VIBROMETER	
	Device 4	Device 6	Device 4	Device 6
Peak height	0.707 μm	0.742 μm	0.636 μm	0.606 μm
Peak width	34 Hz	23 Hz	35 Hz	17 Hz
Quality Factor	131	168	123	214

Table 5. The comparison of two devices in term of peak height width, and quality factor.

D. TRANSIENT TIME OF RESPONSE

The transient responses of the two sensors were simulated using PSPICE the sound incident at 45° . Figures 24 (a) and (b) show the simulated transient data for the Device 6 and 4, respectively.

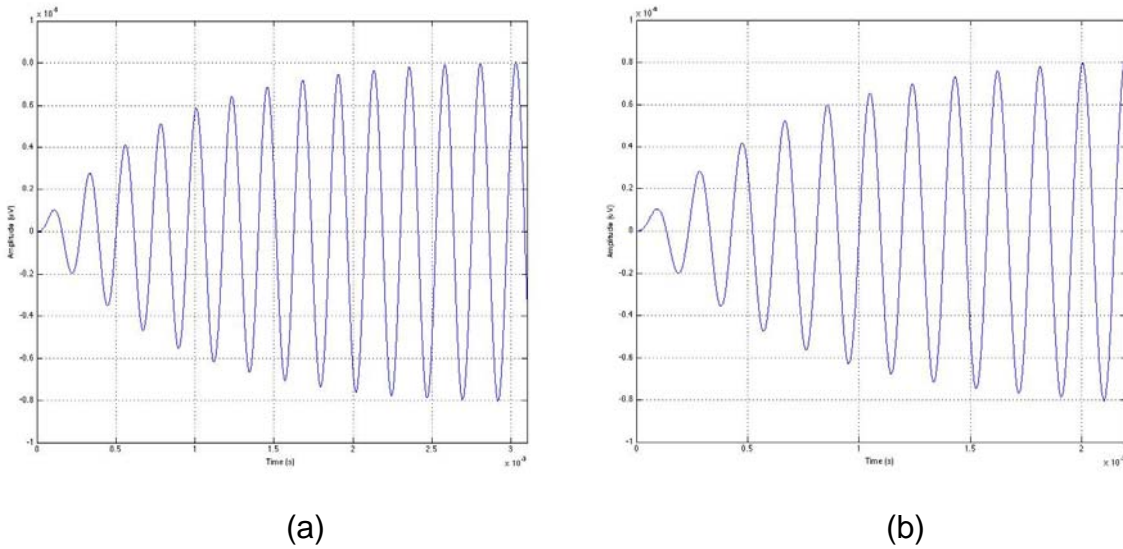


Figure 24. Transient time of response measured by PSPICE. A. Device 6 (solid wings). B. Device 4 (perforated wings).

The data in Figure 24 show that the time required for attaining the steady state response for Device 4 (perforated wings) is about 2.2 ms and for Device 6 (solid plate) is about 3.1 ms. The higher settling time for the Device 4 is due to the smaller damping ratio $\gamma = b/m$. The transient response amplitude of a damped harmonic oscillator is given by (G. Karunasiri, 2009)

$$A(t) = A_0 e^{-\gamma t} \quad (1.31)$$

The lighter mass associated with the structure with perforated wings produce a larger damping ratio making a faster rise of the transient amplitude. In addition, the perforation can increase the damping coefficient (b) making the damping ration higher.

E. ROCKING AND BENDING AMPLITUDE RATIO WITH INCIDENCE ANGLE OF SOUND

In order to determine the directional sensing capability of this system, amplitudes at rocking and bending frequencies were measured for as a function of direction of sound. Figure 25 shows the simulated dependence of ratio of the rocking to bending amplitudes using COMSOL with the incident angle for the two sensors. As expected, the ratio increases with angle due to the increase of the arrival time delay, which increases the rocking amplitude. The rationing was used to remove the unknown sound pressure at the sensor since the increase in time delay does not affect the bending motion.

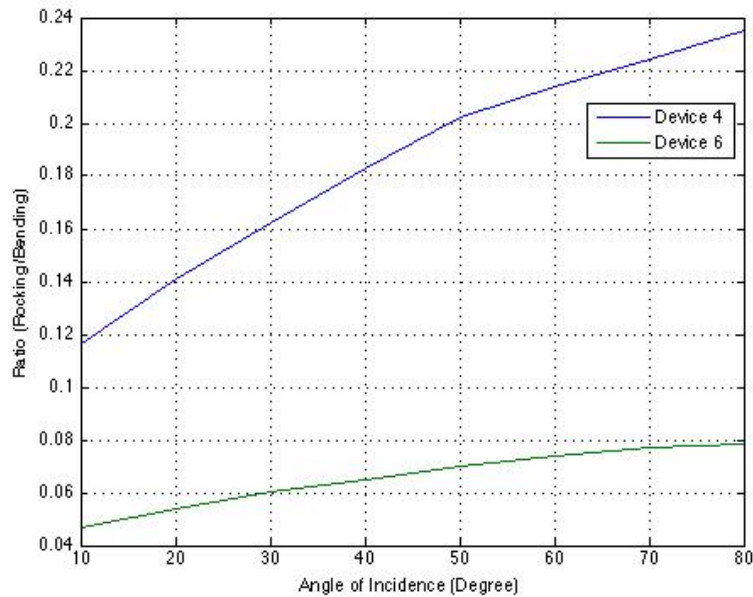


Figure 25. Directional sensitivity of the mechanical response from COMSOL.

The Table 6 shows the measured response for Device 4 (perforated wings) and Device 6 (solid wings), using COMSOL for a number of different incident angles of sound. All the measurements were taken with intensity of sound wave of 0.939 mV/Pa. The increase of the ration with angle agrees well with the simulated data shown in Figure 25.

Phase (°)	DEVICE 4 (perforated wings)			DEVICE 6 (solid wings)		
	Amplitude (μm)		Ratio	Amplitude (μm)		Ratio
	Rocking	Bending	Rocking/Bending	Rocking	Bending	Rocking/Bending
10	0.43	3.7	0.116	0.38	8.15	0.0466
20	0.52	3.7	0.141	0.44	8.15	0.0539
30	0.60	3.7	0.162	0.49	8.15	0.0601
40	0.68	3.7	0.183	0.53	8.15	0.0651
50	0.75	3.7	0.202	0.57	8.15	0.0699
60	0.79	3.7	0.214	0.60	8.15	0.0736
70	0.83	3.7	0.224	0.63	8.15	0.0773
80	0.87	3.7	0.235	0.64	8.15	0.0785

Table 6. Difference in the amplitude of the mechanical response between the tympanal pits for different angles of sound incidence.

V. CONCLUSION

Based on the structure of the auditory system of the fly *Ormia ochracea*, a directional microphone was designed and characterized. It was designed to fabricate using SOIMUMPs the performance was analyzed using COMSOL and PSIPCE software. The main goal of the research was to characterize two identical sensors with solid and perforated wings. It was found that the two sensor had nearly identical response amplitude to sound indicating good sound coupling. The sensor with perforated wings showed less curling due to residual stress compared to the sensor with solid wings. Both sensors showed good sensitivity to the direction of sound. The measured and simulated frequency responses of the sensors showed good agreement. The use of perforated wing allows the increase of damping ratio making the sensor to respond faster and giving a relatively broader frequency response.

THIS PAGE INTENTIONALLY LEFT BLANK

VI. RECOMMENDATIONS FOR FUTURE WORK

For the future work, these experiments need to be done in an anechoic chamber to reduce the interference from unwanted reflection from the walls in the lab.

THIS PAGE INTENTIONALLY LEFT BLANK

LIST OF REFERENCES

- COMSOL, (Version 3.4), (2007). [Computer Software]. www.comsol.com.
- Dritsas, Antonios (2008, June). Characterization of the MEMS directional sound sensor fabricated using the SOIMUMPs process. The thesis paper of the Naval Postgraduate School.
- G. Karunasiri, Sinibaldi. (2009). 'Lecture Notes'. MEMS Class.
- Gibbons C. and R. N. Miles, (2000). Design of a Biomimetic Directional Microphone Diaphragm. *The Journal of the Binghamton, NY 13902-6000*.
- Hedwig, B. (2005). Parasitoid Flies: Exploiting Acoustic Communication for Predation. *PII – Neuroscience, Module M4/Sensory Systems*.
- Kinsler, Lawrence E. (1976). Fundamentals of Vibration. *Fundamentals of Acoustics*, 978-0-471-84789-2.
- Liu, C. (2006). Bulk Micromachining and Silicon Anisotropic Etching. *Foundations of MEMS*, 0-13-147286-0.
- Miles, R.N., D. Robert, and R.R. Hoy. (1995, December). Mechanically coupled ears for directional hearing in the parasitoid fly *Ormia ochracea*. *The Journal of the Acoustical Society of America*, 98, 3059-3070.
- PSPICE, Microelectronic Circuits, 4th edition, (1998), ISBN 0-19-511663-1.
- Roa, S.S. (2003). Mechanical Vibrations, 4th ed. New Jersey: Pearson Education, Inc. 383-399.
- Robert, Daniel (2001, April). Innovative Biomechanics for Directional Hearing in Small Flies. *Laboratory of Bioacoustics, Institute of Zoology, University of Zurich, Switzerland*.
- Shivok Timothy J. (2007, September). MEMS POLYMUMPS-Based miniature microphone for directional sound sensing. *The thesis paper of the Naval Postgraduate School*.
- Wilson, Oscar Bryan (1988). Hydrophones. *Introduction to Theory and Design of Sonar Transducers*, 0-932146-22-8.
- Zhang W. and Turner, Sensors & Actuators A, 134, 594 (2007).

THIS PAGE INTENTIONALLY LEFT BLANK

INITIAL DISTRIBUTION LIST

1. Defense Technical Information Center
Ft. Belvoir, Virginia
2. Dudley Knox Library
Naval Postgraduate School
Monterey, California